SAND2015-2180C

SOLUTION MINING RESEARCH INSTITUTE
105 Apple Valley Circle
Clarks Summit, PA 18411, USA

Telephone: +1 570-585-8092

www.solutionmining.org

Technical Conference Paper

On the Controls of Mixing of Injected Fresh Water Jets with Brine in Salt Caverns: Scaled Flow Visualization Experiments

Jason E. Heath, Martin B. Nemer, David L. Lord, Sandia National Laboratories, Albuquerque, New Mexico, USA

SMRI Spring 2015 Technical Conference
27 – 28 April 2015
Rochester, New York, USA

Solution Mining Research Institute Spring 2015 Technical Conference

Rochester, New York, USA, 27 – 28 April 2015

ON THE CONTROLS OF MIXING OF INJECTED FRESH WATER JETS WITH BRINE IN SALT CAVERNS: SCALED FLOW VISUALIZATION EXPERIMENTS

Jason E. Heath, Martin B. Nemer, and David L. Lord

Sandia National Laboratories, Albuquerque, New Mexico, USA

Abstract

Mixing of injected fresh water with saturated brine in U.S. Strategic Petroleum Reserve salt caverns governs the shape and rates of change of cavern walls due to leaching. Non-uniform and irregular leaching is a major concern of field operations. Oil withdrawal operations normally involve injection of fresh water into brine near the bottom of a cavern to displace the overlying oil out of the cavern. Of special interest are the factors that control well-mixed conditions below the oil-brine interface or possible movement of poorly-mixed fresh water upward that may form an upper bank of fresh water and concomitant leaching. We investigate factors controlling mixing using laboratory scaled-tank experiments with shadowgraph flow visualization. Parameters varied include: momentum via the flow rate of injected fresh water; degree of injected jet impingement on base of tank via placement of injection nozzle; and detachment of upward-traveling fresh water from the injection string. Initial results presented herein compare the relative strength of controls on mixing, especially with regard initial jet spreading and boundary-layer detachment effects from the injection string of the upward-moving fresh water plume.

Key words: Cavern Operation, Cavern Hydraulics, Cavern Dissolution Experiments

Introduction

Injection of “raw” or low-salinity water and associated leaching affects the shape of salt caverns of the U.S. Strategic Petroleum Reserve (SPR). Control of leaching processes is important to produce and maintain desired cavern storage shapes and volumes. In addition to initial solution mining, leaching occurs during remedial leaching programs to create excess storage volume or alter cavern shapes (Weber et al., 2014). Oil withdrawal can entail injection of raw water into brine near the bottom of a cavern with displacement of the overlying oil column through a production string. The different leaching scenarios involve: a variety of string depths for water injection and brine or oil production; injection flow rates; initial and moving locations of the oil-brine interface (OBI); usually low aspect ratio or slender cavern geometries; initial injected water chemistry and physical properties (e.g., temperature and density); and salt cavern chemistry. Unexpected events such as string breaks can occur, which may greatly alter desired cavern shapes (Rudeen et al., 2013). In all cases, mixing of injected low-salinity water with ambient brine in the confined cavern geometry governs the salt saturation index and thus the potential spatial variability and rates of cavern wall dissolution and recession. Incomplete mixing can lead to undesirable caverns shapes including preferential wall recession at the OBI (Lord et al., 2012; Rudeen et al., 2013).

The scenario of injection of low-salinity water into brine, restated in fluid dynamics terms, is that of the penetration of a negatively-buoyant jet into a miscible liquid. Here “negatively buoyant” means that jet momentum and buoyancy act in opposite directions (Philippe et al., 2005). Previous experimental work examined penetration and mixing behavior of high Reynolds number turbulent negatively, positively, and neutrally buoyant jets in wide or slender containers without bottom impingement (Philippe et al., 2005; Voropayev et al., 2012; and Nath et al., 2014); and the vertical impingement and spreading of turbulent

negatively buoyant jets on a horizontal surface with no effects of lateral confinement (Cooper et al., 2007). The previous work typically focuses on the geometry of plumes of the injected jet and entrained fluids using non-dimensional numbers. Voropayev et al. (2012), in addition to characterizing injected and entrained fluid plumes, describe the continued convection of the plumes generated by positively buoyant jets deeper into a slender column; this "deep convection" is driven by buoyancy and is not dominated by the initial jet momentum.

This paper examines mixing dynamics of both non-impinging and impinging negatively buoyant jets in a slender container, for a range of relatively low-to-high Reynolds numbers, by varying the depth of the injection nozzle and the injection flowrate. Of interest are conditions governing well-mixed to poorly-mixed conditions. These scaled laboratory experiments involve shadowgraph flow visualization using distilled water injected into brine with an upper free (air-brine) interface. This work focuses on the mixing of the injected jet and ambient brine near the base of the vessel, with more preliminary observations of the rising deeply convected plumes to the upper air-brine interface. Results indicate, for jet nozzle placement near the base of the vessel, stronger mixing for higher Reynolds number jets with impingement. However, for the relatively low Reynolds numbers, preliminary results suggest that upwardly moving and deeply convected plumes are well mixed by the travel distance to the top of the tank. Only when the injection nozzle is placed near the upper air-brine interface is a bank of poorly-mixed low-salinity water observed.

Methods and Materials

Typical SPR caverns are cylindrical and approximately 700 m (2297 ft) high by 70 m (229.7 ft) diameter, with aspect ratio of 0.1 (Voropayez et al., 2012). Experiments presented herein were conducted within an acrylic rectangular prism tank with square cross section of 10.16 cm × 10.16 cm (4 in × 4 in) and height of 76.2 cm (30 in; Figure 1). A tube for injection was placed through an opening in the top of the tank. The opening prevented pressurization of the upper head space. The brine column height was set to ~ 66 cm (26 in) at the beginning of each fluid injection period, giving an aspect ratio of 0.15. The ratio of injection nozzle diameter to tank diameter was 0.015, which is ~ 3 times that of a typical SPR cavern. Brine was removed from the top of the tank following subsequent tests to maintain the ~ 66 cm column height, and fresh brine was used as necessary to maintain total dilution between tests to <10%.

The first set of results was performed with imaging near the base of the tank with a Phantom high speed camera under shadowgraph optics (Figure 1). Image resolution was 1200 × 1728 pixels, with up to 4058 frames per single experiment. Fifteen nozzle height–flowrate pairs were measured. A Harvard Apparatus PHD-Ultra series syringe pump supplied deionized distilled water into ~23 wt% NaCl solution at rates of 21.0, 52.5, 105.0, 157.5, and 210.0 ml/min (1.28, 3.20, 6.41, 9.61, 12.8 in^3/min), through a 1.55 mm (0.061 in) diameter nozzle. These flowrates, the nozzle diameter, and the injected water properties result in Reynolds numbers of ~300 to ~3000, whereas common production operations at SPR sites have Reynolds number of ~10^6. Our intention is to investigate mixing behavior from relatively low-to-high Reynolds numbers to observe the range in possible poor-to-well mixing plume behavior; future work will include higher Reynolds numbers (although matching the high SPR values is probably not possible in the laboratory and may not be necessary to observe the transition for poor-to-well mixed conditions). Imaging conducted near the base of the tank captured at least the tip of the nozzle at the greatest base-to-nozzle distance of 7.62 cm (3 in). Two opposing walls of the tank were oriented normal to the light path, and the tank was placed on a tilt table for horizontal leveling. Nozzle height was varied at 2.54, 5.08, and 7.62 cm (1, 2, and 3 in) for the five flowrates, constituting the set of 15 nozzle height–flowrate pairs.

For a second group of results, imaging was performed at the top of the air-brine interface, stilled maintained at ~66 cm (26 in). The nozzle height was maintained at 7.62 cm (3 in) from the base of the tank, with measurements at flowrates of 1.0, 5.0, and 21.0 ml/min (0.06, 0.31, and 1.28 in^3/min). A final measurement was performed with nozzle height at 4.87 cm (1.92 in) from the air-brine interface. Image processing and measurements of plume geometry were performed using Matlab.

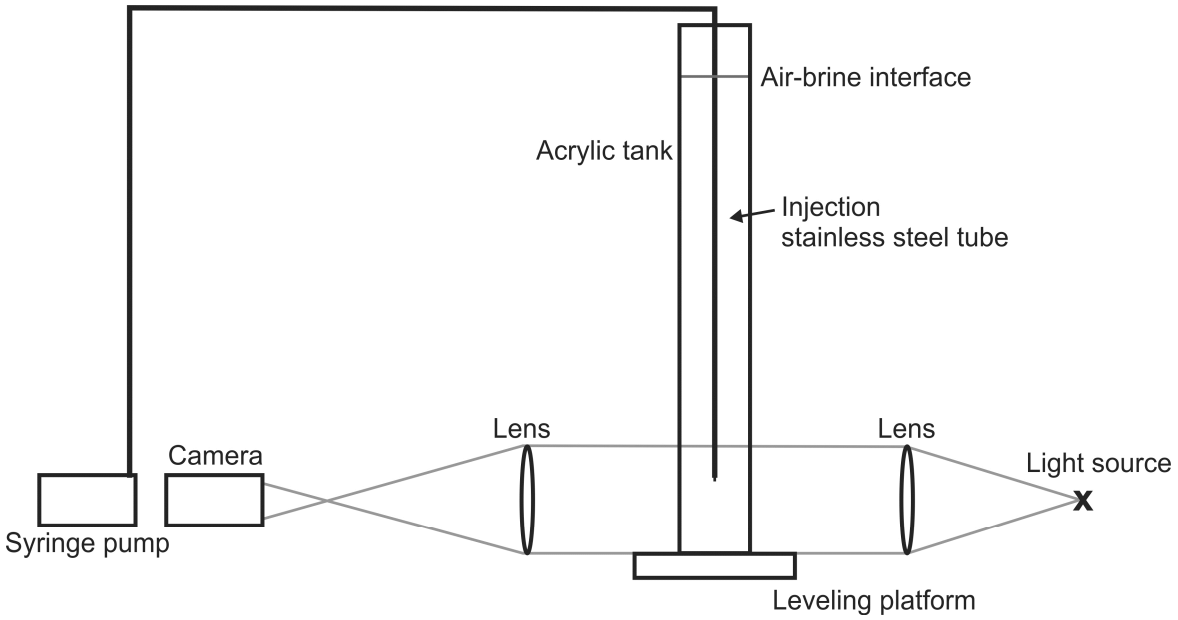

Figure 1. Schematic of the experimental setup for shadowgraph imaging at the base of the tank. Note that for imaging of the air-brine interface, the tank was lowered into the light path.

Results

Figures 2a–c display example image frames for two experiments from the 15 nozzle height–flowrate pairs with imaging at the base of the tank (see Methods and Materials section). Depending on nozzle height and flowrate, plumes of injected water and entrained brine either never touch (or only touch for an initial transient) the vessel base plate (Figure 2b) or impinge on the base plate and spread laterally up to some separation distance that is governed by buoyancy (Figure 2c). Figures 2d–f show results of thresholded grayscale image frames to black and white. Imaging processing to determine nozzle height, the location of the base plate, and the centerline normal distance between base plate and nozzle are shown in Figures 2d–f. Automated image processing measured the plume width normal to the centerline that connects the nozzle to the base plate. For the 15 nozzle height–flowrate pairs, image processing was performed from the start of injection until the approximate time that: 1) circulation of downward moving "deeply convected" plumes enter the field of view at the height of the nozzle (see Figure 3a); or 2) the lateral spreading of the injected and entrained water near the base touches the walls of the vessel (Figure 3b–c). Figure 4 presents examples of plume widths as a function of nozzle-to-base distance and time for non-impinging and impinging cases (such data were collected for all 15 height–flowrate pairs). Each vertical line represents a processed frame. Figure 4a shows that the plume for the flowrate and nozzle height of 52.5 ml/min and 7.77 cm (~ 3 in), respectively, never touches the base plate—the maximum penetration depth is visible from the figure and may be statistically stable after the initial deepest penetration. Both features of the downward moving jet and rising plume are captured by Figure 4a. Figure 4b displays an example of an injection jet that propagates downward and spreads against the base plate for essentially the entire test. The lighter gray values represent the width of the initial downward propagating jet, whereas the overprinting darker values represent the width of the separated and rising buoyant plume.

Figure 5 presents the time-averaged width of the injected plume and entrained brine, between the nozzle and base plate, for all non-impinging cases (cases where the plume does not touch the base plate or only briefly at very early time; see Figures. 2b, 2e, and 4a for examples of non-impingement). By plume, in addition to the downward moving injected and entrained water, we also include the upward moving buoyant water (but not the

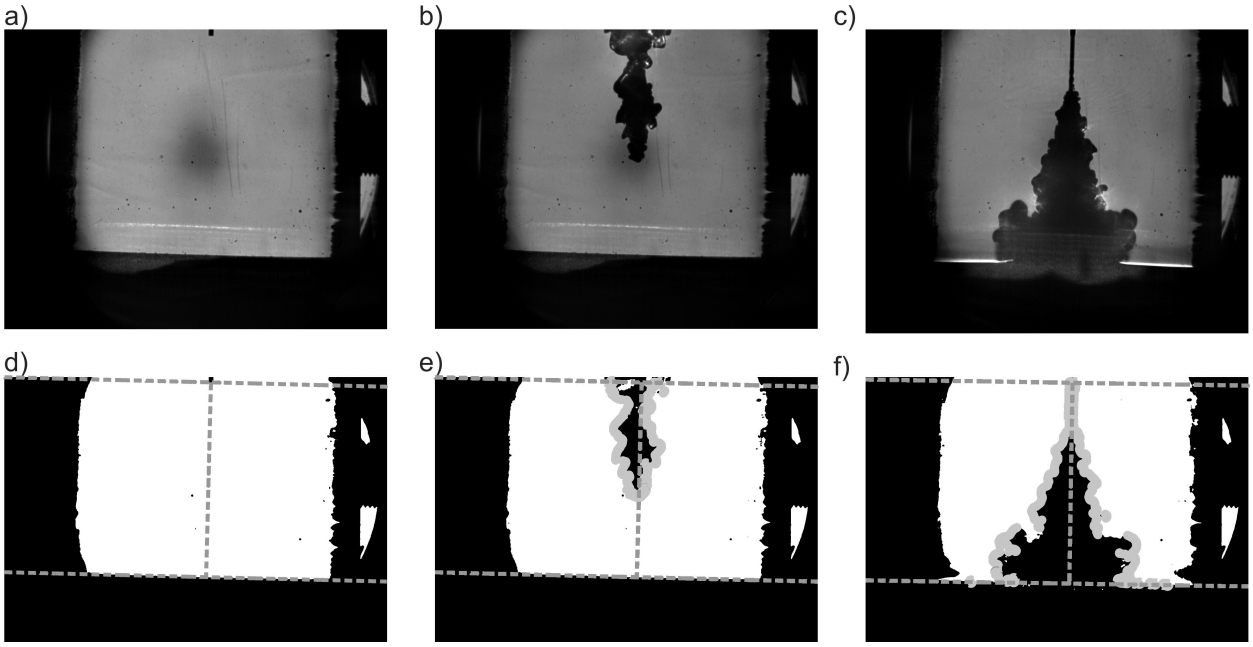

Figure 2. Original and processed shadowgraph images. a) Shadowgraph image of base of tank containing brine prior to injection of deionized distilled water. The injection nozzle is visible at the top center at a height of 7.62 cm. b) Shadowgraph image of injected water at a flowrate of 52.5 ml/min (3.20 in^3/min), which penetrates into the brine column and never impinges against the base plate. c) Shadowgraph image of injected water at flowrate of 157.5 ml/min (9.61 in^3/min), which impinges and spreads against the base plate. d, e, and f) Thresholded versions of Figures 2a, b, and c. Dash lines were calculated by custom image processing algorithms, which determine the location of the base plate and the normal line between the nozzle and the base plate. The gray circles in Parts e and f highlight the margins of the plumes that were identified by the image processing algorithms.

Figure 3. Representative mixing behaviors of the flow imaging experiments at the base of the tank for nozzle height of 7.62 cm (3.0 cm), at the approximate time image processing is stopped. a) The injected water of flowrate 52.5 ml/min (3.20 in^3/min) and entrained plume is clearly visible in the middle as a dark region, surrounded at the top by relatively slow downward moving mixed water. From same data set as Figure 2b. b) The injected water of flowrate 157.5 ml/min (9.61 in^3/min) and entrained plume and buoyant plume are clearly visible. The rising plume touches the wall at the left. c) The injected water of flowrate 210 ml/min (3.20 in^3/min) at the time its rising buoyant plume first touches the side walls.

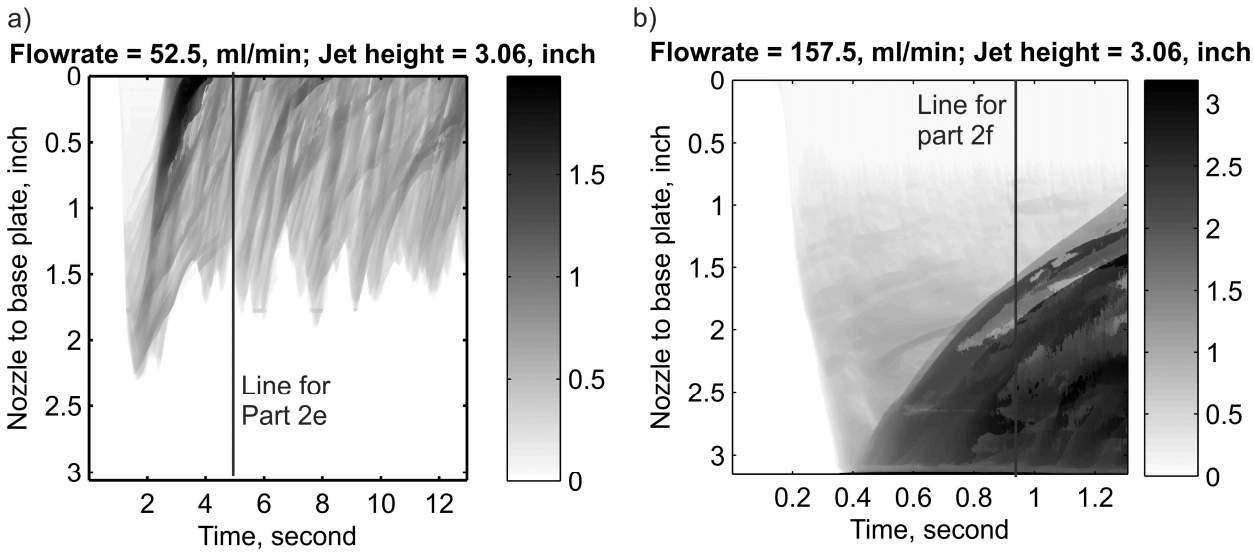

Figure 4. Plume width as a function of the distance between the nozzle and the tank base plate and time. The grayscale colorbar indicates the width of the plumes in inches normal to the centerline that connects the nozzle to the base plate (lines shown in Figures 2e and f). The vertical lines indicate the time at which the image frames for Figures 2e-f were taken.

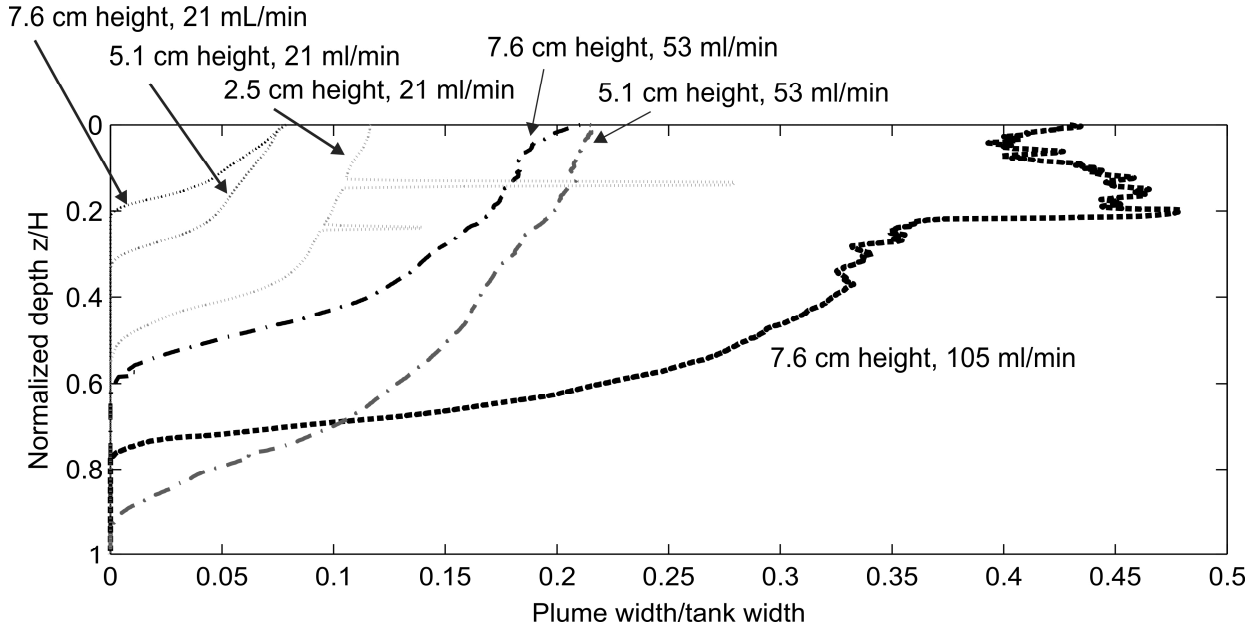

Figure 5. Time-averaged steady-state plume width normalized by tank width versus the distance z from the nozzle towards the base plate normalized by total nozzle-to-base-plate distance. The locations where the curves touch the y axis thus represents the maximum relative (from nozzle to base plate) downward penetration distance of the fluid jet. The locations where the curves touch the x axis represent the maximum width of the rising plume at the depth of the nozzle. Flowrates plotted include 21, 52.5, and 105 ml/min (or 1.28, 3.20, or 6.41 cubic inches/min). The other flowrates from the 15 nozzle height–flowrate pairs exhibit base-plate impingement.

deeply convected mixture, see Figure 3a). Out of the 15 cases, the lower flowrates and higher nozzle heights result in non-impingement, as expected. The case of 7.62 cm (3 in) nozzle height and 105 ml/min exhibits the maximum rising plume and mixing near the nozzle location. The plume width and penetration depth depend strongly on the flow rate. The slopes of the right portions of the curves of Figure 5 indicate the growth of the rising plumes as they travel upward into the tank. The continued growth by the time the plumes reach the upper air-brine interface is of interest to verify well-mixed conditions—imaging at intermediate depths has not be conducted yet to verify the behavior and growth of the rising plumes.

Figure 6 presents the plume width spatially averaged over a 0.25 cm (0.10 in) vertical zone near the bottom of the tank for the cases of injection-jet impingement (see Figures 2c, 3b, and 3c for examples of jets impinging on the base plate). For the 7.62 cm (3 in) nozzle height, the plume width increases with time until the plume begins interacting with the walls of the vessel; the curves exhibit a decreasing-in-magnitude but still positive slope. For the 5.08 cm (2 in) nozzle height, the higher flowrates of 210 and 158 ml/min exhibit changes in slope but positive slopes at later times; however, the 105 ml/min case shows a rise then slight drop to negative slopes with time. The 2.54 cm (1 in) nozzle height cases show positive slopes that essentially become level at later times. These curves reach a steady-state plume width at the base; the progression of sizes is systematic with the lower flowrates having smaller steady-state basal plume widths. Noise in the data of Figure 5 is due to image processing artifacts.

Figure 7 presents the time-averaged (skipping over initial transients) and spatial-averaged (from nozzle exit to bottom of the tank) plume width for all 15 cases as a function of the jet Reynolds number. The injection jet plume width–Re behavior is linear for a given nozzle height up until impingement with the vessel base plate.

Top of tank imaging results for nozzle heights of 7.62 cm (3 inch) above the base of the container show rising, deeply-convected and well-mixed plumes for relatively low flowrates (1, 5, and 21 ml/min; see Figure 8 a-c). We assume higher flowrates will also be well-mixed. Figures 8d-f is the only case that shows the development of a low-salinity bank of stratified water at the top of the tank—this is the case where the nozzle is near the air-brine interface and the flowrate is 1.0 ml/min

Discussion and Future Work

The metric for well-mixed conditions in this study is when the width of the spreading plume of injected and entrained water equals the tank width. The dynamics and conditions of the well-mixed region are a control on leaching of SPR caverns—poorly-mixed low salinity water can lead to irregular leaching. Our results (Figures 2–7) capture important early- to steady-state time behavior of the mixing region near the base of the vessel, for impinging and non-impinging cases, such as the relationship between Reynolds number and plume width (e.g., Figure 7). An important observation is that the initially rising buoyant plumes can still contribute to downward mixing in the confined geometry as shown in Figure 3a. Nozzle height and higher flowrates cause greater mixing of the rising plumes for both impinging and non-impinging cases (see Figures 5–6), suggesting that low flowrates and low nozzle heights might lead to poorly-mixed conditions. However, our results of imaging at the top of the tank indicate that even for low flowrates of 1 ml/min (Figure 8a), corresponding to the nozzle height above the base plate of 7.62 cm (3.0 in), the rising plume appears well mixed. Only when the nozzle is approximately 4.87 cm (1.92 in) from the air-brine interface does a bank of low-salinity fluid form (Figure 8d-f)—such a bank could possibly lead to “undercuts” or preferential leaching at the field scale in a salt cavern. Figures 8d shows the injection nozzle and assembly, which has sharp corners. It appears that boundary-layer fluid detachments occur at the sharp corners that initiate mixing; however, the travel distance is short to the air-brine interface and thus the bank of low-salinity water still forms. We hypothesize that, in the field, fresh water banks may form if upwardly traveling water via boundary layer flow occurs. The boundary layer flow and short travel distances (e.g., due to string breakage) to the OBI thus may lead to ponding of fresh water. Locations of positive curvature on the string may lead to flow detachment and greater mixing. Our continued experiments will examine boundary layer flow along the injection tube with varying degrees of curvature and fluid travel distance to the air-brine interface—to examine how detachment controls mixing. Future work will also include continued dimensional analysis to develop relationships of the controlling factors for the full spectrum of poor-to-well mixed conditions.

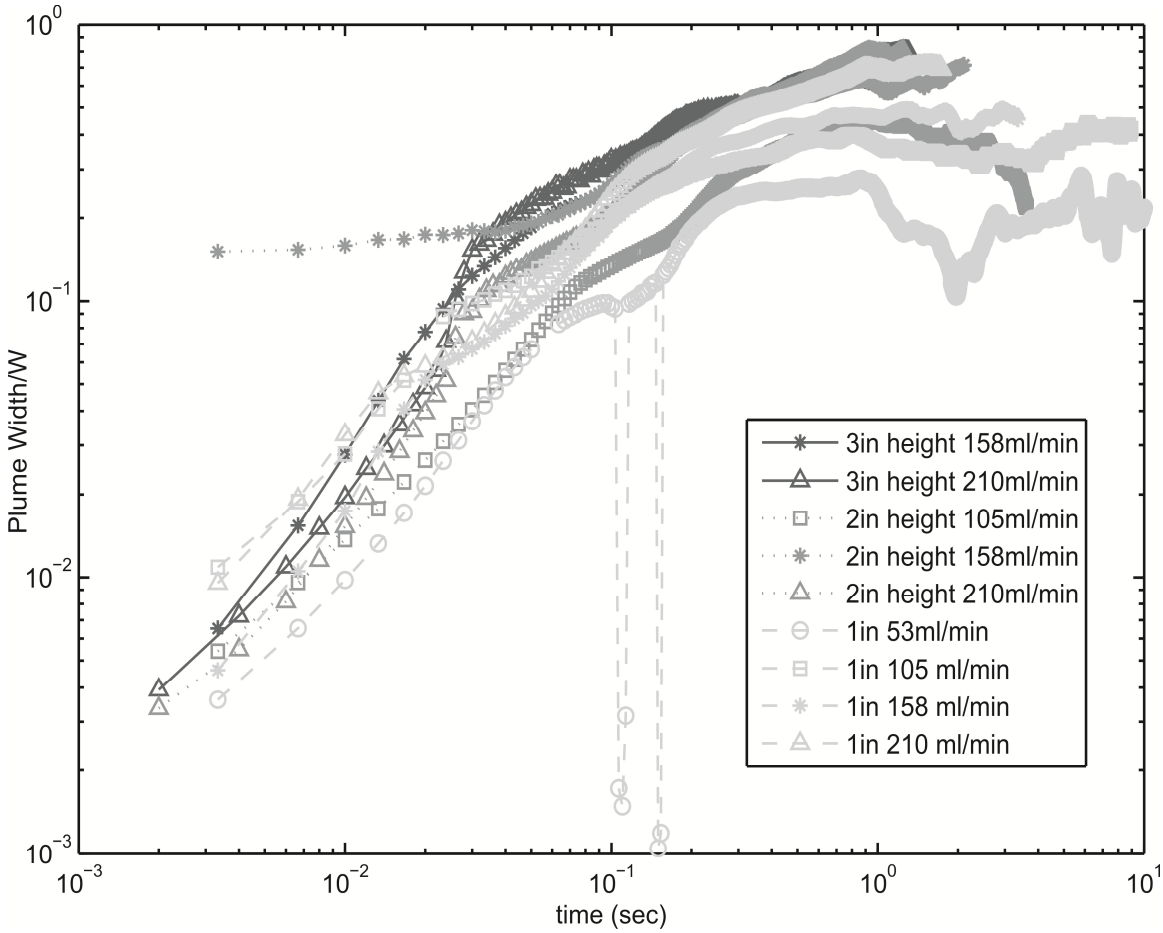

Figure 6. Impinging plume width within ~ 0.25 cm (0.1 in) of the bottom of the tank (normalized by the tank width W) versus time (second).

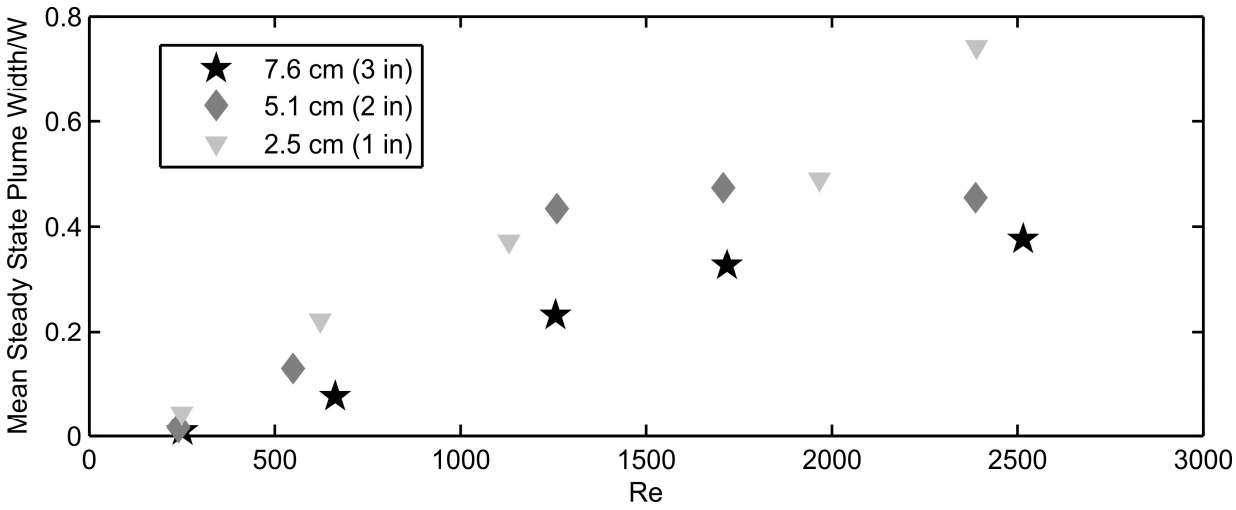

Figure 7. Time averaged and spatial-averaged plume width normalized by the vessel width as a function of the Reynolds number. Notice that plume width is a strong (linear) function of the input momentum for the experiments at lower Re numbers.

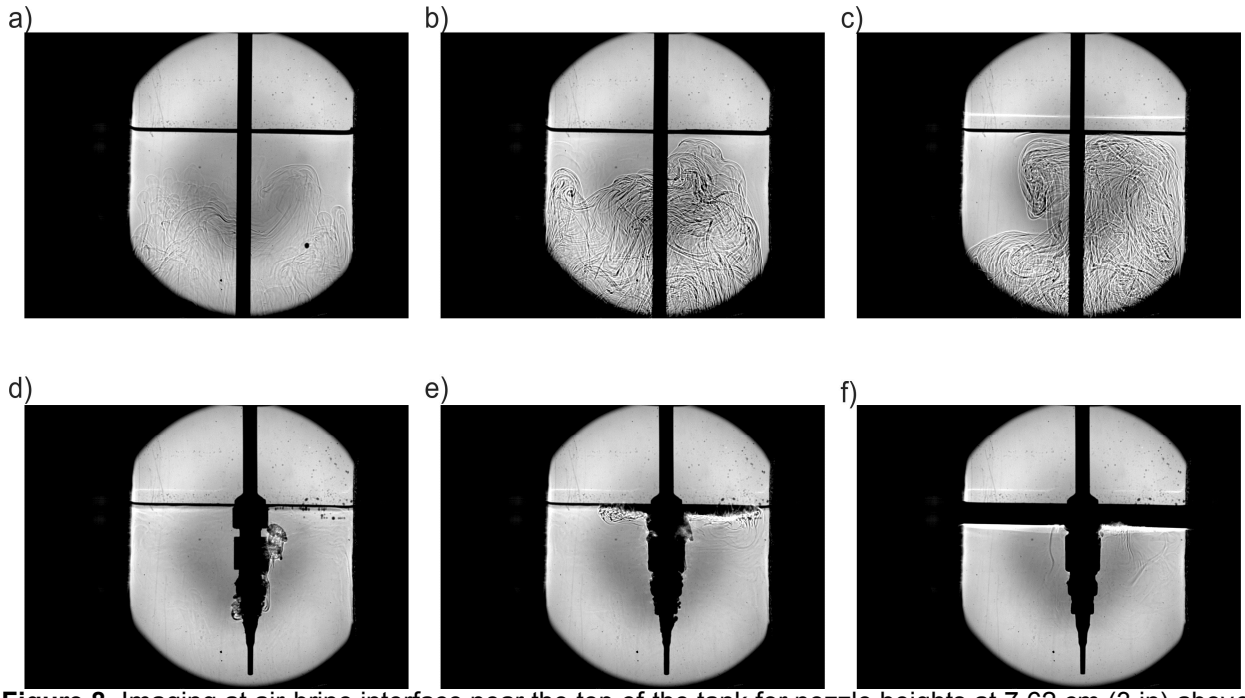

Figure 8. Imaging at air-brine interface near the top of the tank for nozzle heights at 7.62 cm (3 in) above base plate for parts a-c, and ~5.08 cm (~2 in) below air-brine interface for parts d-f. a) Flowrate of 1 ml/min and photo taken after 169.1 s of injection; plume nearly hits interface. b) Flowrate of 5 ml/min and photo taken after 55 s of injection immediately before plume near hits interface.c) Flowrate of 21 ml/min and photo taken after 38 s of injection and immediately after plume hits interface. d-f) Times series of experiments (at 0.5, 17.9 and 169 s) with nozzle near air-brine interface at flowrate of 1 ml/min, which is the only case showing a bank of poorly-mixed water building under the air-brine interface

Acknowledgements

This work was funded by the U.S. Strategic Petroleum Reserve Project, administered by the U.S. Department of Energy. Sandia National Laboratories is a multi-program laboratory managed and operated by Sandia Corporation, a wholly owned subsidiary of Lockheed Martin Corporation, for the U.S. Department of Energy's National Nuclear Security Administration under contract DE-AC04-94AL85000.

References

Cooper, P., Hunt, G.R., 2007. Impinging axisymmetric turbulent fountains. Physics of Fluids 19, 117101.

Lord, D., Roberts, B., Gutierrez, K., Rudeen, D., 2012. Solution mining characteristics of U.S. Strategic Petroleum Reserve oil drawdown. SMRI Spring 2012 Technical Conference, 23–24 April, Regina, Saskatchewan, Canada.

Nath, C., Voropayev, S.I., Lord, D., Fernando, H.J.S., 2014. Offset turbulent jets in low-aspect ratio cavities. Journal of Fluids Engineering 136, DOI: 10.1115/1.4026023.

Philippe, P., Raufaste, C., Kurowski, P., Petitjeans, P., 2005. Penetration of a negatively buoyant jet in a miscible liquid. Physics of Fluids 17, 053601.

Rudeen, D.K., Weber, P.D., Lord, D.L., 2013. Bryan Mound SPR Cavern 113 Remedial Leach Stage 1 analysis. Report No. SAND2013-6185, Sandia National Laboratories, Albuquerque, New Mexico, 43 pp.

Voropayev, S.I., Nath, C., Fernano., H.J.S., 2012. Mixing by turbulent buoyant jets in slender containers. Physics Letters A 376, 3213–3218.

Weber, P., Lord, D., Rudeen, D., 2014. 2014 re-validation of the SANSMIC code. SMRI Spring 2014 Technical Conference, 5–6 May, San Antonio, Texas, USA.